Multiscale assessment of the heterogeneity of scutched flax fibers

Thomas Peyrache, Brigitte Chabbert, Véronique Aguié-Béghin, François Delattre, Bernard Kurek, Angélique Gainvors-Claisse

Multiscale assessment of the heterogeneity of scutched flax fibers

Thomas Peyrache[a], Brigitte Chabbert[a], Véronique Aguié-Béghin[a], François Delattre[b], Bernard Kurek[a], Angélique Gainvors-Claisse[a,*]

[a] Université de Reims Champagne-Ardenne, INRAE, FARE, UMR A 614, AFERE, Reims, France
[b] Université du Littoral Côte d'Opale, UCEIV, UR 4492, Dunkerque, France

* Corresponding author.
E-mail address: angelique.gainvors@univ-reims.fr (A. Gainvors-Claisse)

Abstract

The industrial process of extracting flax fibers from a plant (*Linum usitatissimum* L.), which involves a combination of retting and scutching, could lead to matter heterogeneity within individual roll bales. Although many studies have investigated the variability of flax fiber compositions and properties as functions of various factors throughout the value chain, no researchers have focused on long-fiber bale heterogeneity and its impact on quality. In this work, five batches were empirically identified based on visual and textural criteria, and were subsequently characterized. The study of their differences and similarities using a combination of physicochemical methods allowed them to be classified into several groups, depending on the criteria measured and the structural scale. Thus, variations in surface composition were related to the presence of external tissue residues and microbial biomass but were not related to the measured polysaccharide composition. Additionally, the technical fibers displayed different mechanical and hygroscopic properties, which could be distributed within 2–4 groups, independent of color and surface composition criteria. This study is a first step in determining fiber heterogeneity, which constitutes a global quality assessment for the further application of flax fibers.

Keywords : Flax fiber, Heterogeneity, Mechanical properties, Hygroscopic properties, Physico-chemical analyses

1. Introduction

Flax fibers (*Linum usitatissimum* L.) are among the most widely used plant fibers in the present-day textile and composite industries. Due to their mechanical properties and unique technical characteristics, such as density and hygroscopic properties, these bast fibers are a good alternative to cotton and nonsustainable synthetic fibers (Atav et al., 2023; Sanjay et al., 2018). *In planta*, they are organized as bundles of elementary fibers in the outer part of a stem. Elementary fibers are plant cells approximately 15–25 µm in diameter and 2–5 cm in length that are composed of a thick cell wall of primarily crystalline cellulose, which confers high mechanical properties (Bos et al., 2002; Bourmaud et al., 2013). Furthermore, hemicelluloses and pectins of various types, such as xyloglucans, glucomannans, and rhamnogalacturonans, are present within the primary and secondary cell walls, constituting an amorphous structure that embeds the cellulose microfibrils (Rihouey et al., 2017). The elementary fibers are then held together in bundles by the middle lamella, which is a matrix composed of another type of pectin called homogalacturonans. Besides these various polysaccharides composing the majority of fibers, lignins can also be found in small proportions in the middle lamella and primary cell wall.

In Europe, the extraction process of bast fibers such as flax and hemp fibers involves a pretreatment of the stems in the field; this pretreatment is known as dew retting (Paridah et al., 2011). The aim of this treatment is to degrade the compounds responsible for the cohesion between the fiber bundles and the other tissues of the stem to facilitate the separation of the outer cortical tissues from the inner woody tissues. Moreover, this separation can lead to partial decohesion of the bundles. This degradation is induced by multiple enzymatic activities (Brown et al., 1986; Meijer et al., 1995) originating from microorganisms in the soil and phyllosphere. The complex retting process is directly linked to climatic conditions, which impact the colonization and development of microorganisms on plants laid on the ground in windrows. The process is stopped by human intervention when pectic and hemicellulosic compounds are assumed to be sufficiently hydrolyzed before the degradation of cellulose. The windrows are then collected as straw bales. Fibers are extracted from straw by a mechanical process called scutching. The efficiency of scutching is highly dependent on the degree of retting (Akin et al., 2005), that is the extent of degradation of the middle lamella within the fiber bundle and cell wall constituents of the epidermis and parenchyma surrounding the bundles. Subsequently, technical fibers are recovered in different forms, such as elementary fibers, bundles, and groups of bundles (Barbulée et al., 2014), and packaged in bales of long fibers before entering various transformation chains.

Technical fibers at this stage of scutching are subjected to high variability resulting from several individual and combined key point events that occur throughout the process, from sowing to extraction. In addition to initial genetic factors and agricultural practices (Baley et al., 2020), dew retting is a vital factor that directly impacts the initial mechanical extraction process according to the conditions and equipment used. The variability of the technical fibers occurs at various scales, including composition, morphology, surface finish, and mechanical properties, all of which define the overall quality, which can vary between harvests. The heterogeneity of these parameters within the same industrial bale is also a factor in the overall quality determined, which is an important phenomenon to consider for the valorization of the product. The quality of the fibers obtained after scutching is assessed empirically by farmers (Drieling et al., 2010), who then determine their applicability in various materials, from textiles to composites. Therefore, managing the quality chain and procedure is of critical importance, particularly at the level of retting, as exposure to microorganisms must neither be too short to properly separate different stem tissues nor too long to limit the degradation of cellulose for yield and quality purposes (Djemiel et al., 2020). Many studies have thus investigated the impacts of retting time, the annual and regional variations of retting (Chabbert et al., 2020; Martin et al., 2013; Pisupati et al., 2021), and the mechanical extraction method (Lyu et al., 2021) on fiber quality.

In recent years, climate change has directly impacted flax plant development (Kwiatkowska et al., 2023; Melelli et al., 2022) and dew retting, potentially increasing the heterogeneity of harvests, as noted by farmers through organoleptic methods. Due to the decrease in frequency and increase in volume of rainfall, the management of retting time has become more complex, increasing the difficulty of achieving the desired results. This heterogeneity, which contributes to variability, results in different fiber qualities within the same harvest. To date, estimations of fiber heterogeneity are still empirical at the industrial level, even though some researchers have reported that colorimetry and infrared spectroscopy can provide valuable information for comparing processed flax fibers (Akin et al., 2000; Chabbert et al., 2020; Fernandez-Tendero et al., 2017; Sohn et al., 2004).

The aim of this study was to characterize the heterogeneity of a bale of retted and scutched

flax fibers obtained at an industrial scale. For this purpose, batches of fiber strands were identified empirically, mimicking the organoleptic methods of flax farmers, and were characterized by microscopy and various physicochemical methods widely used for bast fibers. The objective was to assess differences between the identified fibers at different organization levels and determine their resulting mechanical and hygroscopic properties, providing new insights into the heterogeneity and quality of present industrial harvests.

2. Materials and methods

2.1. Materials and sampling

Scutched flax fibers of the Aramis variety, grown in Herbelles (northern France) in 2021, were supplied by Van Robaeys Frères. The fibers were obtained from a windrow several dozen meters long, harvested on the same field, and conditioned into a round 30kg bale which was stored at ambient temperature in a covered shed. These long technical fibers were qualified as "medium" quality by the scutcher based on their organoleptic characteristics. To study the heterogeneity of this commercial round bale, sampling at the laboratory was performed over a length of approximately 1 meter after removal of the first external roll-up (Fig. 1).

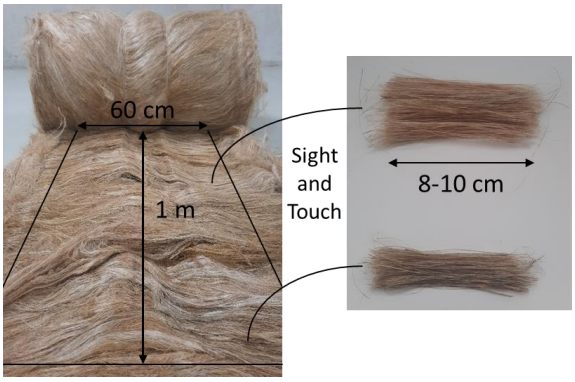

Fig. 1. Sampling area on the fiber bale.

A total of 15 centimeters at each end of the long fibers was cut, and the central part (1 m × 60 cm) was retained, assuming that structural and maturity variabilities in the original stem were reduced (Charlet et al., 2007). Portions of long fibers (strands) that were 8–10 cm in length and as homogeneous as possible were isolated by three operators. This sorting was based on the visual color and fineness to the touch of the fibers to form different batches. To ensure a minimum of heterogeneity within the batches formed, several successive sortings were carried out.

2.2. Macroscopy and scanning electron microscopy imaging

Macroscopic images were obtained using an Axiozoom V16 (Zeiss, Germany) at total magnifications of 7× and 40×. An S80-55 ring light connected to the VisiLED MC 1500 (Schott, Germany) illuminates the samples from the top.

Scanning electron microscopy (SEM) images were acquired with a JSM7100F electron microscope (JEOL, Japan) equipped with three ultrathin-window (30 mm^2) energy-dispersive X-ray spectroscopy (EDS) detectors (XFlash 6/30, Bruker, USA). The fibers were metalized with a thin layer of chrome using a Q150T Plus (Quorum Technologies, UK) for the observations.

2.3. Colorimetry

The color of the fiber strands was measured using a colorimeter (CR-400, Konica Minolta, Japan). The results were expressed according to the CIELab color space, with L* representing the brightness, a* representing the red/green axis, and b* representing the yellow/blue axis. The analysis was conducted in 8 replicates per batch on a surface with an area of 50 mm^2.

2.4. Infrared spectroscopy

Fourier transform infrared (FTIR) analyses were performed on a Nicolet 6700 spectrometer (Thermo Scientific, USA) using attenuated total reflectance (ATR). Each spectrum was acquired using OMNIC software over an average of 32 scans in the spectral region between 4000 and 528 cm^{-1} after background subtraction, with a

resolution of 4 cm^{-1}. Each batch was characterized by a set of 16 spectra recorded at different points on the strands. Spectra were analyzed after baseline correction through 7 points (4000, 3675, 2400, 1800, 1500, 1185, and 825 cm^{-1}) and mean normalization in the 4000–825 cm^{-1} spectral region using Unscrambler software (CAMO, USA).

2.5. Thermogravimetric analysis

Thermogravimetric analysis (TGA) was performed with an SDT650 (TA Instrument, USA) using TRIOS software. Each batch had 6 replicates of cut fibers that weighed approximately 10 mg. The batches were analyzed at reaching 800 °C, increasing by 10 °C/min under a nitrogen flow at 100 mL/min. For each analysis, decomposition temperatures were obtained from the first derivative TGA (DTGA) curve, and the mass losses corresponding to each peak were determined after correction for water loss.

2.6. Monosaccharide analysis

Two methods of fiber acid hydrolysis were performed to determine their monosaccharide compositions. Analyses were performed in triplicate on approximately 5 mg of ground samples. Sulfuric acid hydrolysis was performed with a swelling phase in 125 µL of 12 M acid for 2 h at 20 °C, followed by 1 M sulfuric acid hydrolysis for 2 h at 100 °C (Bleuze et al., 2018). Hydrolysis with 2 M trifluoroacetic acid (TFA) was conducted at 120 °C for 1 h (Crônier et al., 2005). The released monomers were analyzed by high-performance anion-exchange chromatography with pulsed amperometric detection (HPAEC-PAD) on a Dionex ICS 5000^{+} (Thermo Scientific, USA) according to Bleuze et al. (2018).

2.7. Morphological and tensile tests of the technical fibers

Cross-sectional determination and tensile tests were performed consecutively on technical fibers previously conditioned at 20 °C and 50% relative humidity for 24 h. For both measurements, fibers without apparent defects and with heterogeneous diameters were selected under a magnifying glass. Approximately 40 fibers per batch, each 30 mm in length, were attached to plastic tabs with ultraviolet (UV)-curing glue (DYMAX, Germany).

The cross-sectional area was measured at five points on each fiber with a Fibre Dimensional Analysis System (FDAS770, Dia-Stron, UK) over 360°. The equivalent diameter was calculated using an elliptical model (Gogoli et al., 2021), accounting for a maximum and a minimum diameter, the ratio of which determined the shape factor. Based on Garat et al. (2018), each cross-sectional scan was analyzed to identify and remove incorrect values, mainly due to the detachment of the elementary fibers from the main bundle.

Tensile tests were performed on a Linear Extensometer (LEX820, Dia-Stron, UK). The displacement rate was set to 3 mm/min with a data acquisition frequency of 50 Hz. Traction modulus between 0.15% and 0.35% of elongation, stress, and strain at break were recovered for each test.

2.8. Dynamic vapor sorption (DVS)

The hygroscopic properties of the fiber strands were measured using an SPSx-1µ Advance (ProUmid, Germany) with a sample mass of 100–200 mg at 20 °C in a single run with all batches. Two compressed air flows, one wet and one dry, were used to regulate humidity in the enclosure, reaching a total flow rate of 5 L/min. Sorption isotherms were obtained from different steps, starting at 5% relative humidity (RH) and progressing to a 10–90% RH in increments of 10%. Equilibrium was determined by monitoring mass changes every 10 min with a resolution of 1 µg until a plateau was reached (±0.02% over 90 min) after a minimum time of 4 h. Desorption isotherms were measured from 80% to 5% RH using the same increments. To determine the dry masses of the samples necessary to calculate the water content, they were dried at 40 °C for 36 h at the end of the analysis.

The repeatability of the sorption/desorption isotherms was verified at each equilibrium RH by using the ProUmid reference (microcrystalline cellulose). The standard error did not exceed 6% of the mean water content of the sample at 10% RH and 3% between 20% and 90% RH.

2.9. Statistical analysis

Welch's t-tests were used to compare group mean values for each analysis performed at least in triplicate, as the hypothesis of equality of variances was not verified in all instances. Statistical tests were conducted using the free software R at a significance level of 5%.

3. Results

3.1. Sampling characterization: Color, morphology, and appearance

The intrinsic heterogeneity of the scutched fiber bale was first visually evaluated (Fig. 1). The differences observed were mainly based on two criteria: naked eye color, and fineness to the touch assessed by roughness. On this basis, five batches were identified as being different on at least one of the two criteria. At low magnification, batches 1, 2, and 3 appeared lighter than batches 4 and 5 (Fig. 2a). The surfaces of the two latter batches were covered with dark residues, probably composed of microbial biomass visible at high magnification (Fig. 2b, orange arrows). Nevertheless, batches 1–3, which had few of these dark residues, presented some black spots, which qualitatively appeared more frequently on the surfaces of batches 1 and 2 than on batch 3 and smaller than those in batches 4 and 5 (blue arrows). In addition, the presence of residual external tissues or internal tissue marks was observed by SEM imaging in different proportions (Fig. 2c, white and black arrows). The tissues were distributed at the surfaces of the fibers in batches 3 and 5 to a greater extent than in the other three batches.

The technical fiber cross-sections were measured, and the five batches were distributed within four diameter groups according to statistical analysis (Table 1). Batches 1–5 had mean diameters between 83 and 141 µm with no significant differences between batches 3 and 4.

The five empirically isolated batches were distinguished into two groups based on macroscopic observations (light, l, and dark, d) and four diameter levels (small, S, medium, M, large, L, and extra-large, XL). Therefore, the samples were classified as follows from 1 to 5: l-S, l-M, l-L, d-L, and d-XL.

Colorimetric analysis of the CIELab color space showed variations in the three axes between the five batches (Table 1). The L* parameter values ranged from approximately 47 to 63, with significant systematic differences between batches, forming five groups. For parameters a* and b*, the first three batches were significantly different, with values between 3 and 5 and between 15 and 25, respectively. Conversely, the last two batches had similar a* and b* values of 3 and 18, respectively. The three visually light batches differed from each other in terms of their three colorimetric parameters, whereas the two dark batches differed only in terms of their L* values.

Table 1.
Morphological and colorimetric data of the fibers from the five batches. Values with different letters within a column are significantly different at $p \leq 0.05$.

	Diameter (µm)	**L***	**a***	**b***
1 (l-S)	83.1 ± 22.0^{a}	62.70 ± 0.74^{a}	2.84 ± 0.26^{a}	15.45 ± 0.84^{a}
2 (l-M)	101.1 ± 21.6^{b}	61.55 ± 1.28^{b}	4.15 ± 0.35^{b}	21.44 ± 1.26^{b}
3 (l-L)	117.6 ± 22.3^{c}	55.01 ± 1.89^{c}	5.04 ± 0.57^{c}	24.62 ± 1.13^{c}
4 (d-L)	115.5 ± 26.6^{c}	51.97 ± 1.43^{d}	3.46 ± 0.30^{d}	18.03 ± 1.43^{d}
5 (d-XL)	140.9 ± 26.1^{d}	47.24 ± 1.50^{e}	3.39 ± 0.62^{d}	18.63 ± 1.53^{d}

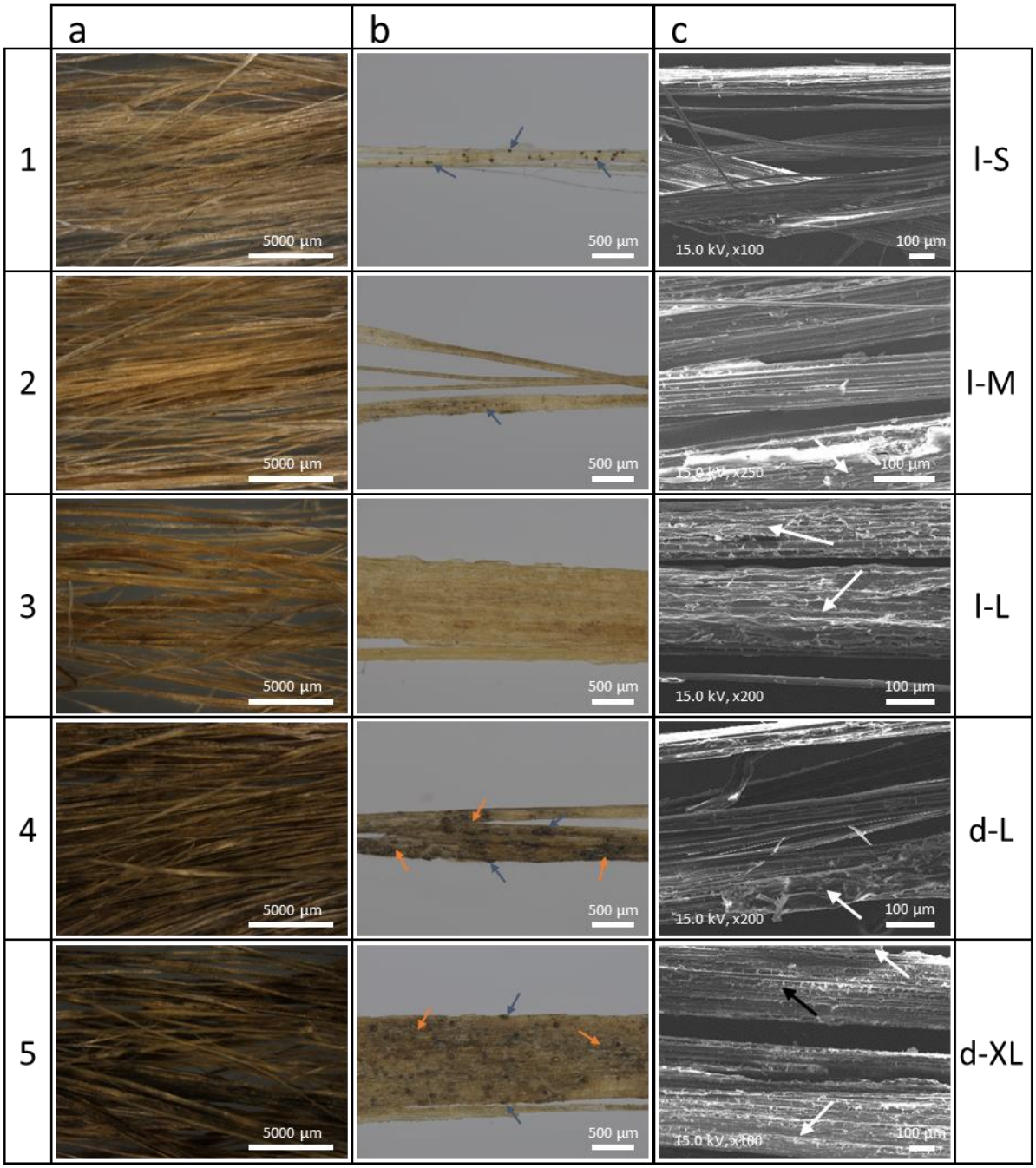

Fig. 2. Observations of the five batches isolated from a bale of scutched flax fibers. Macroscopic images at a) 7× and b) 40× magnification (orange arrow: layer of microorganism residues, blue arrow: dark spots) and c) SEM images (white arrow: external tissues, black arrow: internal tissue marks).

3.2. Infrared analysis

The chemical composition of the fiber surface was determined by FTIR–ATR. The spectra of the first few microns on the fiber surface could be recovered, with a maximum infrared (IR) laser penetration of approximately 2–3 µm at 825 cm^{-1} (Vigoureux, 2003). The average spectrum of 16 spectra recorded at different points on the strands for each batch (Fig. 3) displayed absorption bands that could be attributed to the fiber cell walls (cellulose, hemicelluloses, and pectins) and the cuticle components (cutins, waxes, and phenolic compounds) (Table 2).

Table 2.
Main infrared signals in the 1800–825 cm^{-1} region of the spectra and their classification (Gierlinger et al., 2008; Heredia-Guerrero et al., 2014; Himmelsbach et al., 2002; Zimniewska et al., 2018).

Wavenumber (cm^{-1})	Bond	Assignment
1730–1736	C=O	Pectins, cutins, waxes
1630–1650	O-H	Water
1608–1615	COO	Pectates
1505; 1595	C-C ar.	Lignins
1500–1650	C-C ar.	Phenolic compounds from cuticle
1460–1463; 1472–1473	C-H_2 and C-H_3	Lignins, cutins, waxes, cellulose, hemicelluloses and pectins
1461–1463	O-H	Water
1430	C-H_2	Cellulose
1425–1430	COO	Pectates
1422	C-C ar.	Lignins
1329–1336	O-H	Cellulose, hemicelluloses, lignins and pectins
1312–1317	C-H_2	Cellulose, hemicelluloses
1156–1167	C-O-C	Cellulose, hemicelluloses, pectins, cutins
1100–984	C-O	Cellulose, hemicelluloses, pectins
896	C-O-C	Cellulose, hemicelluloses, pectins

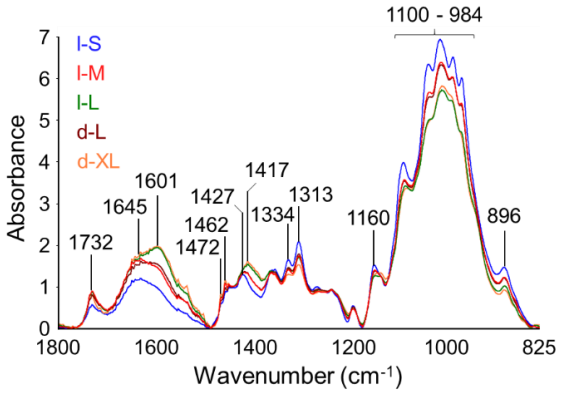

Fig. 3. Average ATR spectra of the five batches in the 1800–825 cm^{-1} region.

The spectra revealed differences in the intensities of the vibration bands mainly between 1800 and 825 cm^{-1}, especially at 1601, 1417, and 1100–984 cm^{-1} (Fig. 3). Principal component analysis of the spectra was then performed to visualize possible differences between batches (Fig. 4a). The score plot of the PC1 axis, representing 79% of the total variation, opposed two spectral regions, one from 1800 to 1370 cm^{-1} and the other from 1370 to 825 cm^{-1} (Fig. 4b). The spectra of the l-L and d-XL batches were localized in the negative part of PC1, indicating the highest intensity in the 1800–1370 cm^{-1} region, as shown at bands at 1732, 1601 and 1417 cm^{-1}. Conversely, the spectra of the l-S batch were in the positive part showing that these fibers displayed the highest intensity of the bands between 1370 and 825 cm^{-1} compared to those of the other batches. Finally, the infrared signals of the l-M and d-L batches were close to the origin, forming a third group between the two described above.

3.3. Thermal analysis

The DTGA curve showed different fiber decomposition stages (Fig. 5) after an initial water loss between 30 and 175 °C. The first decomposition between 200 and 270 °C was attributed to hemicelluloses and pectins, the second between 270 and 380 °C was attributed to cellulose, and the third above 400 °C was attributed to char decomposition (Chabbert et al., 2020; Mazian et al., 2018).

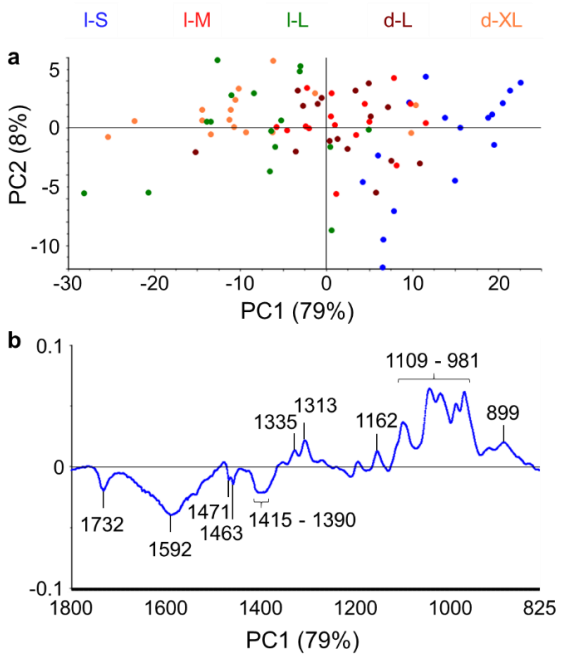

Fig. 4. Principal component analysis of the 1800–825 cm^{-1} region of the infrared spectra: a) score plot (PC1/PC2) and b) PC1 loading.

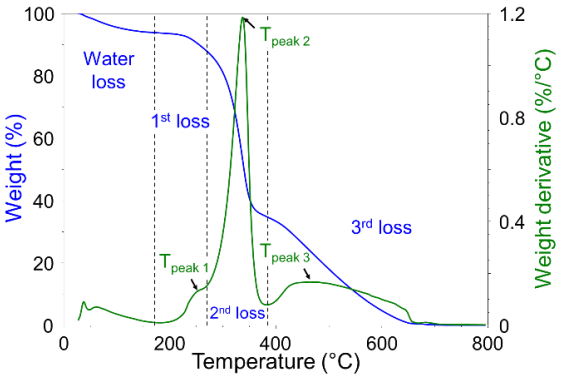

Fig. 5. Characteristic TGA and DTGA curves for the fibers in this study.

The temperature corresponding to the first decomposition ($T_{peak\ 1}$) was greater for the l-S batch (271 °C) than for the d-L and l-M (265 and 262 °C) and d-XL and l-L (257 and 253 °C) batches, forming three groups (Table 3). Although T_{peak1} was not significantly different at 5% (p = 0.072), the l-M and d-XL batches were classified into distinct groups. Based on the associated decomposition percentage, this peak represented 3.9–4.0% of the total mass of both the l-S and l-M batches and 4.6–4.7% of the total mass of both the d-L and d-XL batches. The decomposition temperature attributed to cellulose ($T_{peak\ 2}$) followed the same pattern as that of T_{peak1}, with the highest value for the l-S batch (349 °C) and the lowest values for l-L and d-XL batches (333 to 336 °C). The percentage decomposition of this second decomposition stage represented approximately 61% for the l-S and l-M batches, compared to 58% for batches l-L, d-L, and d-XL.

3.4. Monosaccharide composition

Sulfuric acid hydrolysis was performed to determine the overall monosaccharide composition of the fibers (Table 4). The proportion of total sugars in l-S (90% dry matter) was greater than that in d-XL (87%) and l-L (83%). The sugar composition, expressed as a percentage of total sugar released, indicated that the proportion of nonglucose in the light batches was significantly lower (10%) than that in the two dark batches (12%).

Table 3.
Thermal properties of the technical fibers.

	$T_{peak\ 1}$ (°C)	Mass loss (%)	$T_{peak\ 2}$ (°C)	Mass loss (%)	$T_{peak\ 3}$ (°C)	Mass loss (%)
l-S	270.8 ± 2.9^{a}	4.0 ± 0.2^{a}	349.0 ± 3.4^{a}	61.2 ± 0.9^{a}	501.8 ± 6.8^{a}	34.5 ± 0.5^{a}
l-M	262.1 ± 4.2^{bc}	3.9 ± 0.2^{a}	341.8 ± 3.3^{bc}	60.1 ± 0.5^{b}	483.0 ± 16.4^{ab}	35.1 ± 0.8^{a}
l-L	253.3 ± 4.8^{d}	4.2 ± 0.4^{ab}	332.6 ± 6.7^{d}	57.5 ± 1.5^{c}	485.7 ± 7.8^{b}	37.4 ± 1.4^{b}
d-L	264.6 ± 3.8^{b}	4.7 ± 0.3^{b}	343.8 ± 3.9^{b}	58.1 ± 0.6^{c}	483.9 ± 14.2^{ab}	36.3 ± 0.7^{b}
d-XL	256.5 ± 4.8^{cd}	4.6 ± 0.3^{b}	335.5 ± 6.6^{cd}	56.9 ± 1.6^{c}	478.4 ± 15.5^{ab}	36.5 ± 1.0^{b}

Table 4.
Monosaccharide compositions of the technical fibers determined by sulfuric acid hydrolysis (as % dry matter and % total monosaccharides ± standard deviation). NGlc: sum of monosaccharides other than glucose.

	Total	Glc	NGlc
	% dry matter	% total monosaccharides	
l-S	90.1 ± 0.6[a]	90.1 ± 0.3[ab]	9.9 ± 0.2[ab]
l-M	89.1 ± 1.4[ab]	90.2 ± 0.1[a]	9.8 ± 0.1[a]
l-L	83.1 ± 0.3[c]	89.9 ± 0.1[b]	10.1 ± 0.1[b]
d-L	88.9 ± 0.9[a]	88.4 ± 0.1[c]	11.6 ± 0.1[c]
d-XL	86.5 ± 0.5[b]	88.6 ± 0.1[c]	11.4 ± 0.1[c]

Table 5.
Monosaccharide compositions of the technical fibers determined by trifluoroacetic acid hydrolysis (as % total monosaccharides ± standard deviation).

	Glc	Ara + Rha + GalA + Xyl	Gal + Man
l-S	61.0 ± 0.2[a]	12.8 ± 0.4[a]	25.1 ± 0.2[a]
l-M	53.3 ± 0.1[b]	19.4 ± 0.0[b]	25.4 ± 0.2[a]
l-L	53.2 ± 1.1[b]	21.2 ± 0.5[c]	23.1 ± 0.2[b]
d-L	47.0 ± 0.3[c]	20.8 ± 0.3[c]	30.9 ± 0.2[c]
d-XL	46.1 ± 0.2[d]	23.1 ± 0.1[d]	29.1 ± 0.2[d]

3.5. Tensile properties of the technical fibers

The use of a 30-mm gauge length, similar to the average length of elementary fibers, enabled the estimation of mechanical properties involving the fiber–fiber interfaces in a fiber bundle (Beakou & Charlet, 2013; Singhal et al., 2023). Fig. 6 shows the traction modulus, shape factor, and stress and strain at break values for each batch. The highest traction modulus was determined for the fibers from the l-L batch (22.1 GPa) and was significantly greater than the values obtained for those from the l-S and l-M batches (16.0 GPa) and d-XL (13.9 GPa). Fibers from the d-L batch had a modulus (18.9 GPa) that was significantly greater than that of those from the d-XL batch. The shape factor, which is the ratio between the maximum and minimum diameters, was greater in the l-L batch (2.9) than in the other batches (2.1 to 2.3). This difference mainly arose due to the relatively high values for l-L fibers with diameters greater than 120 µm, whereas no such variation was observed for the fibers with diameters smaller than this value (Supplementary Data). Finally, the stress and strain at break values of the l-S fibers were significantly lower than those of the other fibers (284 vs. 494 to 607 MPa and 1.64 vs. 2.41 to 2.45%), thus constituting two groups.

3.6. Hygroscopic properties

Fig. 7 shows the fiber sorption and desorption isotherms and the associated hysteresis curves. The differences in the moisture contents of the five batches were mainly observed above 60% RH. Three groups were observed in the following order from the most to the least hygroscopic: d-XL, l-L and d-L, and l-M and l-S (Fig. 7a). Hysteresis between desorption and sorption curves, related to the retention of water molecules, displayed a similar pattern in all five batches, with a maximum at 60% RH. However, four groups could be identified where the highest maximal hysteresis was obtained for d-XL fibers (1.53%), whereas the lowest maximal hysteresis was determined for l-S fibers (1.27%) (Fig. 7b).

4. Discussion

The aim of this study was to characterize the visual and textural heterogeneity of an industrial roll bale of retted flax fibers after extraction. This heterogeneity was determined to be inherent in natural fiber harvests and critically contributed to the quality management process within various

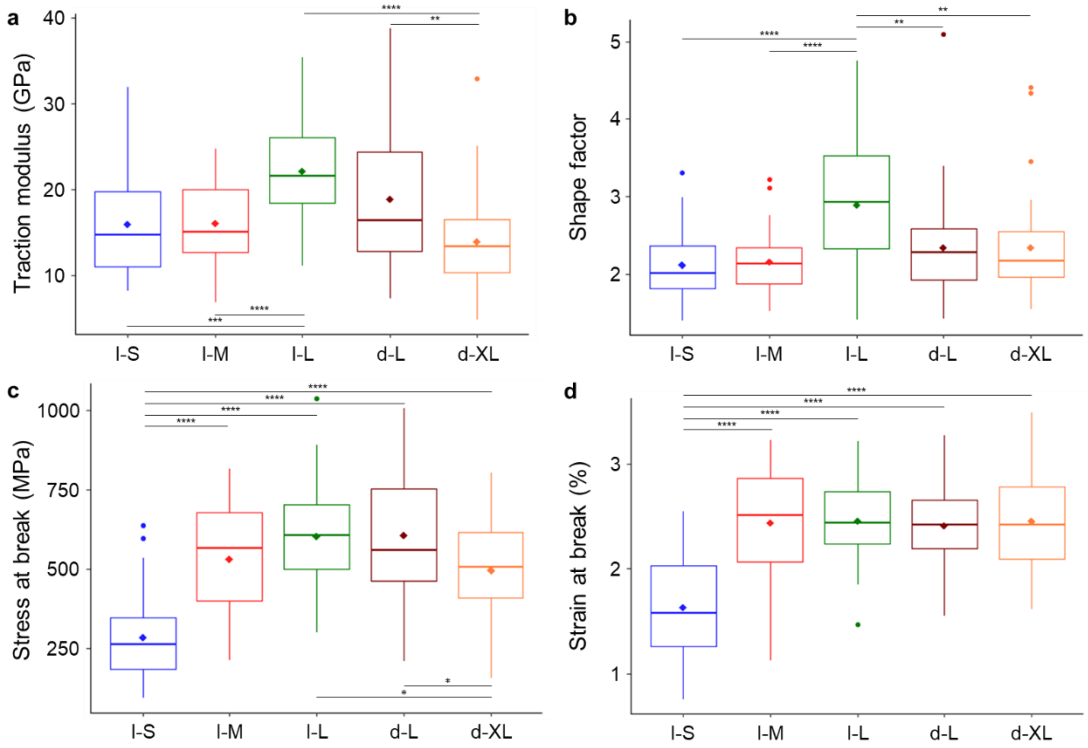

Fig. 6. Box plots of the a) traction modulus, b) shape factor, c) stress at break, and d) strain at break values of the technical fibers. Box plot legend: line = median, dot = mean. Outliers (colored dots outside the boxes) were taken into account in statistical analyses. $p < 0.05$ (*), $p < 0.01$ (**), $p < 0.001$ (***), and $p < 0.0001$ (****) indicate significant differences.

value chains. Therefore, the use of quantitative measurements appeared necessary for the development of new applications. For this purpose, five empirically selected fiber batches were subjected to extensive physicochemical analyses to evaluate the key properties of these fibers and map their differences and similarities.

The five batches selected empirically according to their visual color and fineness to the touch were characterized according to the selection parameters. At the macroscopic level, the fibers from the five batches could be classified into five color groups, as evidenced by the distinct brightness parameter L* (Table 1). The determination of the fiber diameters revealed differences, and the fibers could be divided into four distinct groups. The light fibers l-S and l-M had small and medium sizes, whereas the dark fibers d-L and d-XL had large and extra-large sizes.

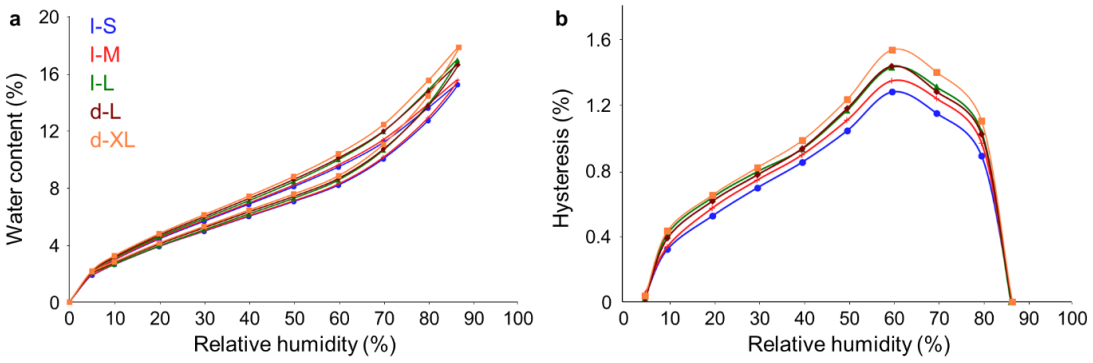

Fig. 7. a) Sorption–desorption isotherms and b) desorption–sorption hysteresis of the technical fibers.

However, l-L and d-L fibers had similar mean diameters, although all color parameters were distinct, suggesting no clear relationship between these two factors. The color variations could be explained by the different surface appearances of the fibers, which were directly visible to the naked eye. In particular, the d-L and d-XL batches were similar to the retted fibers reported to have a characteristic gray-like color due to microbial colonization during retting (Fig. 2a and b) (Martin et al., 2013; Mazian et al., 2018). Although not quantified, the presence of external tissue residues resulting from partial separation of the fibers within the stem during scutching could contribute to the color (Fig. 2c).

The fiber surface was comprehensively characterized using infrared spectroscopy, a method widely used on plant fibers (Fernandez-Tendero et al., 2017; Lupoi et al., 2014; Marcuello et al., 2023; Zimniewska et al., 2018). In particular, analysis of the ATR spectra revealed variations in the band intensities in the 1800–1370 cm^{-1} region, which could be partially attributed to aromatic compounds and pectates for flax fibers, and in the 1370-825 cm^{-1} region, which corresponded to polysaccharides (cellulose, hemicelluloses, and pectins) (Fig. 4b and Table 2). This analysis revealed three groups, among which batches l-L and d-XL had similar surface compositions regarding the highest content of pectin-rich middle lamella and cuticle compounds, although they differed in diameter and color (Fig. 4a). Since there are few lignins in flax fibers, and no characteristic band was visible at 1505 cm^{-1}, the stronger signals at 1601 and 1417 cm^{-1} in l-L and d-XL batches could be partially assigned to pectate-rich epidermal cells (Jauneau et al., 1997), given the abundance of external tissue residues on their surfaces (Fig. 2c). In contrast, the surface of the l-S batch, which had a strong signal between 1100 and 896 cm^{-1}, was primarily composed of cellulose. This finding was in agreement with the SEM images. Variation in the presence of microorganisms was observed by macroscopic imaging (Fig. 2b) and could contribute to infrared differences between fibers. However, the characteristic infrared spectral bands shown in microorganisms (Chirman & Pleshko, 2021; Girometta et al., 2020) were not clearly detected at 1540 cm^{-1} (amide II) and did not show variations between the fiber batches.

Since the composition and structural organization of the fibers governed the main mechanical characteristics and the hygroscopic properties of the technical fibers, analyses of the thermal degradation (Chabbert et al., 2020; Martin et al., 2013; Mazian et al., 2018; Placet et al., 2017) and sugar composition (Gautreau et al., 2022; Rihouey et al., 2017) were conducted. TGA mainly revealed the variations in the temperature of the first decomposition ($T_{peak\ 1}$), which were attributed to hemicelluloses and pectins (Table 3), forming three groups independent of diameter and color. According to the overall monosaccharide analyses, the dark batches (d-L and d-XL) were characterized by a greater proportion of nonglucose sugars than the light batches (Table 4). Similarly, analyzing the polysaccharide amorphous components using TFA hydrolysis revealed an increased proportion of Man+Gal in the d-L and d-XL batches (Table 5). This change could reflect the presence of microbial biomass on the lignocellulosic material (Bertrand et al., 2009), as observed in Fig. 2b, given that some fungal walls contained polysaccharides, such as galactans and mannans (Chakraborty et al., 2021). Finally, considering the proportions of monosaccharides constituting the middle lamella and the primary cell wall (Ara+Rha+GalA+Xyl), the fibers could be distributed into four groups. Notably, the distribution patterns of the five batches within the four groups were the same in terms of the presence of the latter polysaccharides and diameters, suggesting a relationship between these two parameters.

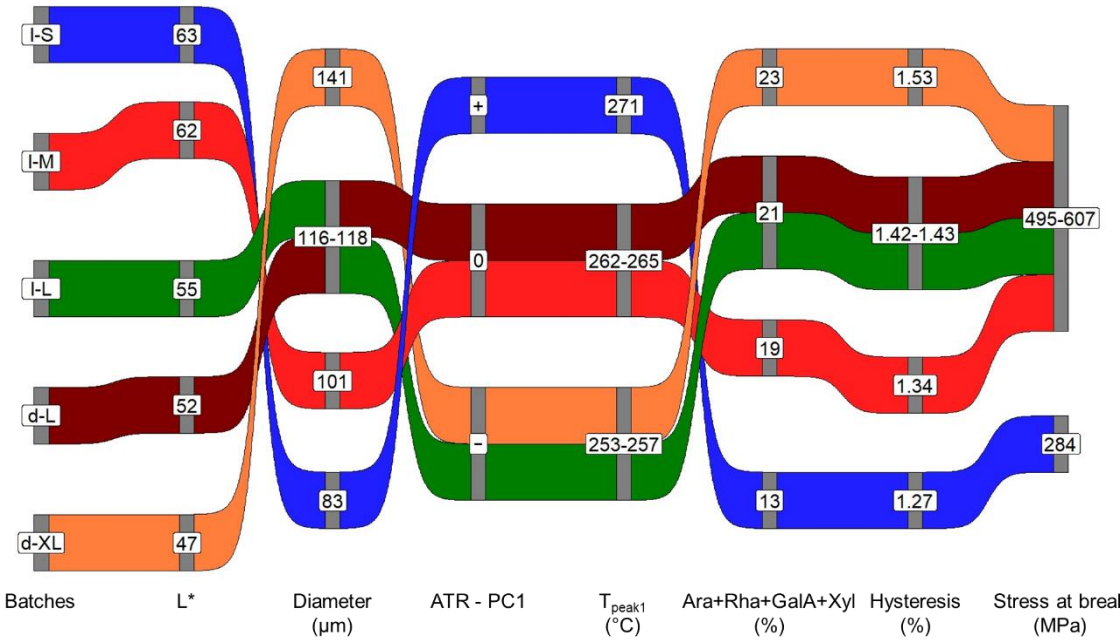

Fig. 8. Grouping of fiber batches according to analyses at different scales. One discriminating parameter per analysis: CIELab L* parameter, diameter (µm), position of point cloud on PC1 axis after PCA on ATR spectra (+: positive, 0: origin, -: negative), T_{peak1} value from TGA (°C), sum of arabinose, rhamnose, galacturonic acid, and xylose after TFA hydrolysis (% total monosaccharides), desorption-sorption hysteresis (%), stress at break (MPa). Values in the labels correspond to the means for each parameter. Batches grouped on the same grey node are not statistically different. The distance between each node of the same parameter is proportional to the difference in mean values, according to a vertical axis (bottom: lowest value, top: highest value). Figure generated under R.

The results from the empirical separation into five batches showed different levels of heterogeneity according to the scales of analysis and the parameters considered. Fig. 8 shows the different groupings based on one parameter per analysis, highlighting that batches with similar surface chemistry could be different in diameter or sugar composition. It is therefore possible to observe similar groupings between surface analysis (PCA, ATR) and thermal analysis (T_{peak1}, TGA) performed on the overall matter. Accounting for macroscopic and microscopic observations, the initial heterogeneity of the fiber bale quantified by the various methods employed (color, infrared, TGA, and acid hydrolysis) could be partially related to residual compounds not originating from the fiber (cortical tissues and microorganisms) and the proportions and compositions of noncellulosic compounds in the fibers. Thus, the d-XL batch corresponded to groups of bundles still retaining external tissue residues, while the l-S batch corresponded to refined bundles, given their respective diameters, surface compositions, and aspects, suggesting a greater degree of cleanliness. These differences could have occurred due to different local conditions of retting along a stem, such as its contact with retting microorganisms or its position in the windrows.

The hygroscopic and mechanical tensile properties of technical fibers are among the most important parameters to manage during a qualification process for further valorization. Regarding hygroscopic properties, water sorption/desorption isotherms and associated hysteresis were used to distinguish three and four groups, respectively (Fig. 7). The greater proportion of sugars associated with the middle lamella and primary cell wall (Ara+Rha+GalA+Xyl)

in the large batches (l-L, d-L, d-XL) than in the small batches (Table 5) could contribute to the increase in the maximum amount of water sorbed after 60% RH because these amorphous compounds were more hydrophilic than crystalline cellulose (Célino et al., 2014). Given that the diameter was in agreement with the relative proportion of the middle lamella and primary cell wall and that the fiber structure influenced water diffusion, the increase in either the mass proportion of these compounds or in the diameter could account for the increased retention of water molecules on thick technical fibers, which was visible through the hysteresis amplitude. In terms of tensile properties, very few significant differences appeared between batches, except for the relatively high traction modulus determined for l-L fiber batch, which also had large shape factor (Figs. 6a, b). Another notable difference is the weakness of the l-S fibers compared to the other fibers, as shown by their relatively low breaking properties (Figs. 6c, d). This phenomenon could be explained by the high cellulose content of these fibers (highest $T_{peak\ 2}$ and associated mass loss) and the low contents in the middle lamella and primary cell wall (lowest Ara+Rha+GalA+Xyl content). The role of middle lamella has been underlined in tensile properties at the bundle scale (Gautreau et al., 2022). In addition, the 15–30% increase in the relative proportion of glucose obtained after TFA hydrolysis of the l-S fibers indicated increasingly amorphous cellulose. This change could result from an alteration of the cellulose structure by microorganisms during retting, impacting the tensile properties of the technical fibers, as previously reported (Nuez et al., 2022). Finally, the data obtained showed an increase in traction modulus with increasing fineness on each batch, which was in agreement with the typical observations of different technical fibers (Baley et al., 2020). However, the finest batches (l-S and l-M) were not those with the highest mechanical properties, reflecting differences between batches at equivalent diameters (Supplementary Data).

The variations in composition measured previously impacted the usual properties of these fibers. In terms of the mechanical properties, only l-S diverged from the others by accounting for the entirety of each batch with different diameters. Considering these differences in diameter and the possible differences in technical fiber morphology (bundles and groups of bundles), the batches differed, mainly in terms of traction modulus. Although the hygroscopic properties differed above 60% RH, they were similar under ambient conditions (approximately 50% RH) where the fibers could be used in regard to water sorption. However, differences were noted in water retention, another property of usage. In addition to their physicochemical properties, the morphology and surface composition varied between batches. All these characteristics were considered important in the final use of the fibers, indicating different qualities and potentially distinct behaviors during the processing steps following scutching, such as combing and carding (Lyu et al., 2021).

5. Conclusions

The industrial process of extracting flax fibers from stems was strongly linked to the combination of retting and scutching, which could induce heterogeneity.

The results highlighted the simultaneous presence of fibers exhibiting various ranges of heterogeneity, considering the different levels of organization, from their surface aspect to their constitutive polymer, and considering their mechanical and hygroscopic properties.

The various methods used enabled the mapping of the heterogeneity of this industrial batch, with some criteria emerging that could be quantified. The L* parameter of the CIELab colorimetric space, as well as the infrared signals, were particularly discriminating criteria regarding surface composition, which could be evaluated quickly and non-destructively. However, these criteria were not related to differences in hygroscopic and mechanical properties,

emphasizing that quantitative assessment of fiber quality required in-depth studies to establish trends between the constituent parameters of heterogeneity.

Understanding this heterogeneity to effectively manage it is perhaps one method for improving quality chain processes, requiring sorting upstream of processing lines based on key parameters that had to be identified in the future.

CRediT authorship contribution statement

Thomas Peyrache: Writing – original draft, Visualization, Investigation, Formal analysis. **Brigitte Chabbert:** Writing - review & editing, Validation, Supervision, Conceptualization. **Véronique Aguié-Béghin:** Writing – review & editing, Validation. **François Delattre:** Writing – review & editing, Conceptualization. **Bernard Kurek:** Writing - review & editing, Conceptualization. **Angélique Gainvors-Claisse:** Writing – review & editing, Supervision, Funding acquisition, Conceptualization.

Funding

This work was supported by the University of Reims Champagne Ardenne and Region Grand-Est through a PhD grant; and Grand Reims.

Acknowledgements

The authors thank Van Robaeys Frères (France) for providing flax samples and technical support from the FARE laboratory: François Gaudard for chemical analysis, Miguel Pernes for DVS analysis, and Anouck Habrant for support with macroscope imaging.

References

Akin, D. E., Dodd, R. B., & Foulk, J. A. (2005). Pilot plant for processing flax fiber. *Industrial Crops and Products*, *21*(3), 369-378. https://doi.org/10.1016/j.indcrop.2004.06.001

Akin, D. E., Epps, H. H., Archibald, D. D., & Sharma, H. S. S. (2000). Color Measurement of Flax Retted by Various Means. *Textile Research Journal*, *70*(10), 852-858. https://doi.org/10.1177/004051750007001002

Atav, R., Dilden, D. B., Keskin, S., & Ergünay, U. (2023). Investigation of the dyeability and various performance properties of fabrics produced from flax and hemp fibres and their blends with cotton in comparison with cotton. *Coloration Technology*. https://doi.org/10.1111/cote.12720

Baley, C. (2002). Analysis of the flax fibres tensile behaviour and analysis of the tensile stiffness increase. *Composites Part A: Applied Science and Manufacturing*, *33*(7), 939-948. https://doi.org/10.1016/S1359-835X(02)00040-4

Baley, C., Gomina, M., Breard, J., Bourmaud, A., & Davies, P. (2020). Variability of mechanical properties of flax fibres for composite reinforcement. A review. *Industrial Crops and Products*, *145*, 111984. https://doi.org/10.1016/j.indcrop.2019.111984

Barbulée, A., Jernot, J.-P., Bréard, J., & Gomina, M. (2014). Damage to flax fibre slivers under monotonic uniaxial tensile loading. *Composites Part A: Applied Science and Manufacturing*, *64*, 107-114. https://doi.org/10.1016/j.compositesa.2014.04.024

Beakou, A., & Charlet, K. (2013). Mechanical properties of interfaces within a flax bundle—Part II : Numerical analysis. *International Journal of Adhesion and Adhesives*, *43*, 54-59. https://doi.org/10.1016/j.ijadhadh.2013.01.013

Bertrand, I., Prevot, M., & Chabbert, B. (2009). Soil decomposition of wheat internodes of different maturity stages : Relative impact of the soluble and structural fractions. *Bioresource Technology*, *100*(1), 155-163. https://doi.org/10.1016/j.biortech.2008.06.019

Bleuze, L., Lashermes, G., Alavoine, G., Recous, S., & Chabbert, B. (2018). Tracking the dynamics of hemp dew retting under controlled environmental conditions. *Industrial Crops and Products*, *123*, 55-63. https://doi.org/10.1016/j.indcrop.2018.06.054

Bos, H. L., Van Den Oever, M. J. A., & Peters, O. C. J. J. (2002). Tensile and compressive properties of flax fibres for natural fibre reinforced composites. *Journal of Materials Science*, *37*(8), 1683-1692. https://doi.org/10.1023/A:1014925621252

Bourmaud, A., Morvan, C., Bouali, A., Placet, V., Perré, P., & Baley, C. (2013). Relationships between micro-fibrillar angle, mechanical properties and biochemical composition of flax fibers. *Industrial Crops and Products*, *44*, 343-351. https://doi.org/10.1016/j.indcrop.2012.11.031

Brown, A. E., Sharma, H. S. S., & Black, D. L. R. (1986). Relationship between pectin content of stems of flax cultivars, fungal cell wall-degrading enzymes and pre-harvest retting. *Annals of Applied Biology*, *109*(2), 345-351. https://doi.org/10.1111/j.1744-7348.1986.tb05326.x

Célino, A., Freour, S., Jacquemin, F., & Casari, P. (2014). The hygroscopic behavior of plant fibers : A review. *Frontiers in Chemistry*, *1*. https://doi.org/10.3389/fchem.2013.00043

Chabbert, B., Padovani, J., Djemiel, C., Ossemond, J., Lemaître, A., Yoshinaga, A., Hawkins, S., Grec, S., Beaugrand, J., & Kurek, B. (2020). Multimodal assessment of flax dew retting and its functional impact on fibers and natural fiber composites. *Industrial Crops and Products*, *148*, 112255. https://doi.org/10.1016/j.indcrop.2020.112255

Chakraborty, A., Fernando, L. D., Fang, W., Dickwella Widanage, M. C., Wei, P., Jin, C., Fontaine, T., Latgé, J.-P., & Wang, T. (2021). A molecular vision of fungal cell wall organization by functional genomics and solid-state NMR. *Nature Communications*, *12*(1), 6346. https://doi.org/10.1038/s41467-021-26749-z

Charlet, K., Baley, C., Morvan, C., Jernot, J. P., Gomina, M., & Bréard, J. (2007). Characteristics of Hermès flax fibres as a function of their location in the stem and properties of the derived unidirectional composites. *Composites Part A: Applied Science and Manufacturing*, *38*(8), 1912-1921. https://doi.org/10.1016/j.compositesa.2007.03.006

Chirman, D., & Pleshko, N. (2021). Characterization of bacterial biofilm infections with Fourier transform infrared spectroscopy : A review. *Applied Spectroscopy Reviews*, *56*(8-10), 673-701. https://doi.org/10.1080/05704928.2020.1864392

Crônier, D., Monties, B., & Chabbert, B. (2005). Structure and Chemical Composition of Bast Fibers Isolated from Developing Hemp Stem. *Journal of Agricultural and Food Chemistry*, *53*(21), 8279-8289. https://doi.org/10.1021/jf051253k

Djemiel, C., Goulas, E., Badalato, N., Chabbert, B., Hawkins, S., & Grec, S. (2020). Targeted Metagenomics of Retting in Flax : The Beginning of the Quest to Harness the Secret Powers of the Microbiota. *Frontiers in Genetics*, *11*. https://www.frontiersin.org/journals/genetics/articles/10.3389/fgene.2020.581664

Drieling, A., Müssig, J., Graupner, N., Müssig, J., Piotrowski, S., & Carus, M. (2010). Economic Aspects. In *Industrial Applications of Natural Fibres* (p. 49-86). John Wiley & Sons, Ltd. https://doi.org/10.1002/9780470660324.ch3

Fernandez-Tendero, E., Day, A., Legros, S., Habrant, A., Hawkins, S., & Chabbert, B. (2017). Changes in hemp secondary fiber production related to technical fiber variability revealed by light microscopy and attenuated total reflectance Fourier transform infrared spectroscopy. *PLOS ONE*, *12*(6), e0179794. https://doi.org/10.1371/journal.pone.0179794

Garat, W., Corn, S., Le Moigne, N., Beaugrand, J., & Bergeret, A. (2018). Analysis of the morphometric variations in natural fibres by automated laser scanning : Towards an efficient and reliable assessment of the cross-sectional area. *Composites Part A: Applied Science and Manufacturing*, *108*, 114-123. https://doi.org/10.1016/j.compositesa.2018.02.018

Gautreau, M., Durand, S., Paturel, A., Le Gall, S., Foucat, L., Falourd, X., Novales, B., Ralet, M.-C., Chevallier, S., Kervoelen, A., Bourmaud, A., Guillon, F., & Beaugrand, J. (2022). Impact of cell wall non-cellulosic and cellulosic polymers on the mechanical properties of flax fibre bundles. *Carbohydrate Polymers*, *291*, 119599. https://doi.org/10.1016/j.carbpol.2022.119599

Gierlinger, N., Goswami, L., Schmidt, M., Burgert, I., Coutand, C., Rogge, T., & Schwanninger, M. (2008). In Situ FT-IR Microscopic Study on Enzymatic Treatment of Poplar Wood Cross-Sections. *Biomacromolecules*, *9*(8), 2194-2201. https://doi.org/10.1021/bm800300b

Girometta, C., Dondi, D., Baiguera, R. M., Bracco, F., Branciforti, D. S., Buratti, S., Lazzaroni, S., & Savino, E. (2020). Characterization of mycelia from wood-decay species by TGA and IR spectroscopy. *Cellulose*, *27*(11), 6133-6148. https://doi.org/10.1007/s10570-020-03208-4

Gogoli, K., Gehring, F., Poilâne, C., & Morales, M. (2021). Analysis of morphological variations of flax fibre bundles by Fraunhofer diffraction. *Industrial Crops and Products*, *171*, 113856. https://doi.org/10.1016/j.indcrop.2021.113856

Heredia-Guerrero, J. A., Benítez, J. J., Domínguez, E., Bayer, I. S., Cingolani, R., Athanassiou, A., & Heredia, A. (2014). Infrared and Raman spectroscopic features of plant cuticles : A review. *Frontiers in Plant Science*, *5*. https://www.frontiersin.org/articles/10.3389/fpls.2014.00305

Himmelsbach, D. S., Khalili, S., & Akin, D. E. (2002). The use of FT-IR microspectroscopic mapping to study the effects of enzymatic retting of flax (Linum usitatissimum L) stems. *Journal of the Science of Food and Agriculture*, *82*(7), 685-696. https://doi.org/10.1002/jsfa.1090

Jauneau, A., Quentin, M., & Driouich, A. (1997). Micro-heterogeneity of pectins and calcium distribution in the epidermal and cortical parenchyma cell walls of flax hypocotyl. *Protoplasma*, *198*(1), 9-19. https://doi.org/10.1007/BF01282126

Kwiatkowska, E., Zimniewska, M., Przybylska, P., & Romanowska, B. (2023). Effect of Drought Stress on Quality of Flax Fibres. *Materials*, *16*(10), Article 10. https://doi.org/10.3390/ma16103752

Lupoi, J. S., Singh, S., Simmons, B. A., & Henry, R. J. (2014). Assessment of Lignocellulosic Biomass Using Analytical Spectroscopy : An Evolution to High-Throughput Techniques. *BioEnergy Research*, *7*(1), 1-23. https://doi.org/10.1007/s12155-013-9352-1

Lyu, P., Zhang, Y., Wang, X., & Hurren, C. (2021). Degumming methods for bast fibers—A mini review. *Industrial Crops and Products*, *174*, 114158. https://doi.org/10.1016/j.indcrop.2021.114158

Marcuello, C., Chabbert, B., Berzin, F., Bercu, N. B., Molinari, M., & Aguié-Béghin, V. (2023). Influence of Surface Chemistry of Fiber and Lignocellulosic Materials on Adhesion Properties with Polybutylene Succinate at Nanoscale. *Materials*, *16*(6), Article 6. https://doi.org/10.3390/ma16062440

Martin, N., Mouret, N., Davies, P., & Baley, C. (2013). Influence of the degree of retting of flax fibers on the tensile properties of single fibers and short fiber/polypropylene composites. *Industrial Crops and Products*, *49*, 755-767. https://doi.org/10.1016/j.indcrop.2013.06.012

Mazian, B., Bergeret, A., Benezet, J.-C., & Malhautier, L. (2018). Influence of field retting duration on the biochemical, microstructural, thermal and mechanical properties of hemp fibres harvested at the beginning of flowering. *Industrial Crops and Products*, *116*, 170-181. https://doi.org/10.1016/j.indcrop.2018.02.062

Meijer, W. J. M., Vertregt, N., Rutgers, B., & van de Waart, M. (1995). The pectin content as a measure of the retting and rettability of flax. *Industrial Crops and Products*, *4*(4), 273-284. https://doi.org/10.1016/0926-6690(95)00041-0

Melelli, A., Durand, S., Alvarado, C., Kervoëlen, A., Foucat, L., Grégoire, M., Arnould, O., Falourd, X., Callebert, F., Ouagne, P., Geairon, A., Daniel, S., Jamme, F., Mauve, C., Gakière, B., Bourmaud, A., & Beaugrand, J. (2022). Anticipating global warming effects : A comprehensive study of drought impact of both flax plants and fibres. *Industrial Crops and Products*, *184*, 115011. https://doi.org/10.1016/j.indcrop.2022.115011

Nuez, L., Durand, S., Melelli, A., Berrin, J.-G., Haon, M., Drula, E., Beaugrand, J., D'Arras, P., Bourmaud, A., & Baley, C. (2022). Exploring the impact of Verticillium wilt disease on the mechanical properties of elementary flax (Linum usitatissimum L.) fibres. *Industrial Crops and Products*, *182*, 114900. https://doi.org/10.1016/j.indcrop.2022.114900

Paridah, M. T., Ahmed, A., SaifulAzry, S., & Ahmed, Z. (2011). Retting process of some bast plant fibres and its effect on fibre quality : A review. *BioResources*, *6*, 5260-5281. https://doi.org/10.15376/biores.6.4.5260-5281

Pisupati, A., Willaert, L., Goethals, F., Uyttendaele, W., & Park, C. H. (2021). Variety and growing condition effect on the yield and tensile strength of flax fibers. *Industrial Crops and Products*, *170*, 113736. https://doi.org/10.1016/j.indcrop.2021.113736

Placet, V., Day, A., & Beaugrand, J. (2017). The influence of unintended field retting on the physicochemical and mechanical properties of industrial hemp bast fibres. *Journal of Materials Science*, *52*(10), 5759-5777. https://doi.org/10.1007/s10853-017-0811-5

Rihouey, C., Paynel, F., Gorshkova, T., & Morvan, C. (2017). Flax fibers : Assessing the non-cellulosic polysaccharides and an approach to supramolecular design of the cell wall. *Cellulose*, *24*(5), 1985-2001. https://doi.org/10.1007/s10570-017-1246-5

Sanjay, M. R., Madhu, P., Jawaid, M., Senthamaraikannan, P., Senthil, S., & Pradeep, S. (2018). Characterization and properties of natural fiber polymer composites : A comprehensive review. *Journal of Cleaner Production*, *172*, 566-581. https://doi.org/10.1016/j.jclepro.2017.10.101

Singhal, A., Jin, J., Banu, M., & Taub, A. (2023). Effect of enzyme retting conditions on bast bundle differentiation and mechanical properties of flax technical fibers. *Industrial Crops and Products*, *205*, 117478. https://doi.org/10.1016/j.indcrop.2023.117478

Sohn, M., Barton, F. E., Morrison, W. H., & Akin, D. E. (2004). Prediction of Shive Content in Pilot Plant Processed Flax by near Infrared Reflectance Spectroscopy. *Journal of Near Infrared Spectroscopy*, *12*(4), 251-257. https://doi.org/10.1255/jnirs.432

Vigoureux, J. (2003). De l'onde évanescente de Fresnel au champ proche optique. *Annales de la Fondation Louis de Broglie*, *28*(3-4), 525-548.

Zimniewska, M., Rozańska, W., Gryszczynska, A., Romanowska, B., & Kicinska-Jakubowska, A. (2018). Antioxidant Potential of Hemp and Flax Fibers Depending on Their Chemical Composition. *Molecules : A Journal of Synthetic Chemistry and Natural Product Chemistry*, *23*(8), 1993. https://doi.org/10.3390/molecules23081993

Supplementary Data

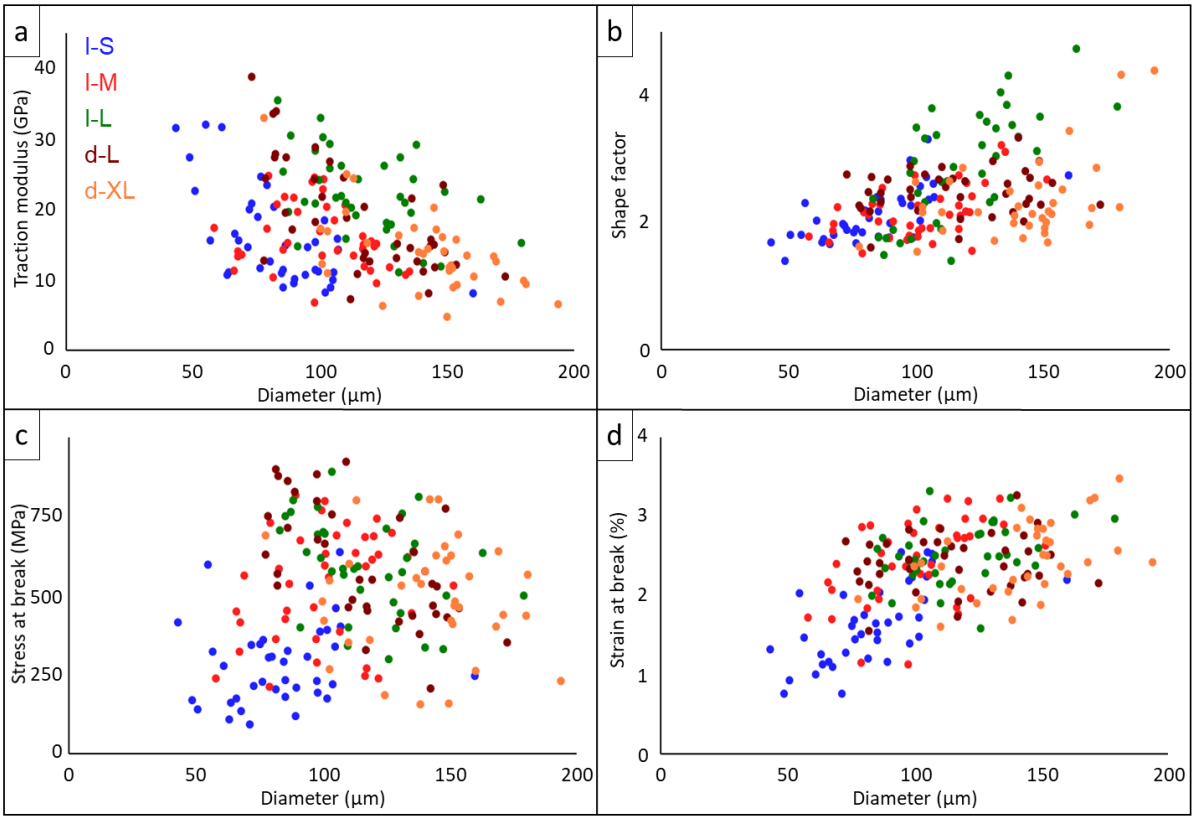

Figure S1. Graphs of the a) traction modulus, b) shape factor, c) stress at break, and d) strain at break of the different batches as a function of diameter.

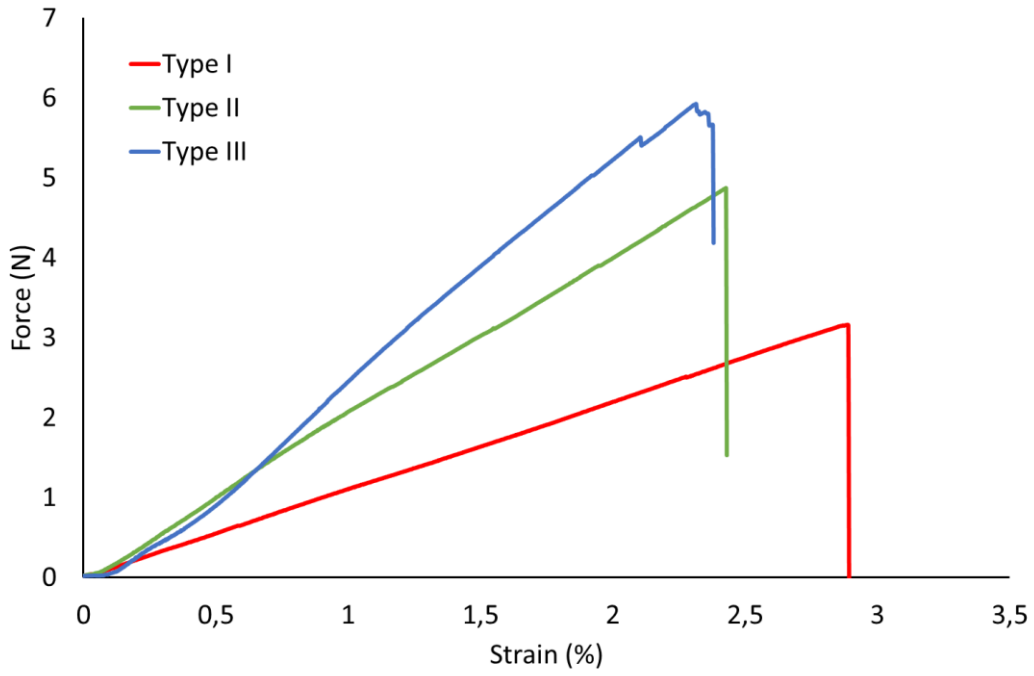

Figure S2. Different shapes of force-elongation curves in this study.